Eur Biophys J (2008) 37:281–294
DOI 10.1007/s00249-008-0261-8

REVIEW

Applications of electron paramagnetic resonance to studies of neurological disease

John F. Boas · Simon C. Drew · Cyril C. Curtain

Received: 2 October 2007 / Revised: 18 December 2007 / Accepted: 21 December 2007 / Published online: 7 February 2008

Abstract Electron paramagnetic resonance spectroscopy (EPR) has the potential to give much detail on the structure of the paramagnetic transition ion coordination sites, principally of Cu^{2+}, in a number of proteins associated with central nervous system diseases. Since these sites have been implicated in misfolding/mis-oligomerisation events associated with neurotoxic molecular species and/or the catalysis of damaging redox reactions in neurodegeneration, an understanding of their structure is important to the development of therapeutic agents. Nevertheless EPR, by its nature an in vitro technique, has its limitations in the study of such complex biochemical systems involving self-associating proteins that are sensitive to their chemical environment. These limitations are at the instrumental and theoretical level, which must be understood and the EPR data interpreted in the light of other biophysical and biochemical studies if useful conclusions are to be drawn.

Keywords Electron paramagnetic resonance · Copper ions · Neurodegeneration · Alzheimer's disease · Parkinson's disease · Prion diseases

Australian Society for Biophysics Special Issue: Metals and Membranes in Neuroscience, held in Melbourne on 11 July 2007.

J. F. Boas (✉) · S. C. Drew · C. C. Curtain
School of Physics, Monash University, Clayton, VIC 3800, Australia
e-mail: john.boas@sci.monash.edu.au

S. C. Drew · C. C. Curtain
Department of Pathology and Bio21 Molecular Biology and Biotechnology Institute, University of Melbourne, Melbourne, VIC 3010, Australia

Abbreviations

α-Sn	α-synuclein
AD	Alzheimer's disease
APP	Amyloid precursor protein
DEPC	Diethylpyrocarbonate
EPR	Electron paramagnetic resonance
ENDOR	Electron nuclear double resonance
ESEEM	Electron spin echo envelope modulation
ESR	Electron spin resonance
EXAFS	Extended X-ray absorption fine structure
NMR	Nuclear magnetic resonance
PB	Scheme of Peisach and Blumberg (1974)
PD	Parkinson's disease
PrP	Prion protein
ROS	Reactive oxygen species

Introduction

The transition metal ions Cu^{2+}, Fe^{3+} and Zn^{2+} occur at total dry weight concentrations of 70, 340, and 350 μM, respectively, in the neocortical parenchyma of healthy brain (Ehmann et al. 1986), although in the amyloid plaque deposits associated with AD their concentrations may reach 0.4 and 1.0 mM for Cu and Fe/Zn, respectively (Lovell et al. 1998), suggesting a severe dysregulation in their homeostasis. The coordination of these metals has been linked variously to their role in promoting peptide aggregation to form the amyloid plaques characteristic of AD, the amyloid fibrils implicated in PD and the prion diseases, in the production of cytotoxic ROS and in causing potentially cytotoxic interactions with cell membranes. Although dramatic evidence of transition metal dysregulation is not as evident in neurodegenerative diseases other

than AD, evidence of ROS-induced damage is found in PD and prion diseases such as scrapie in sheep and Creutzfeld-Jacob disease in humans.

APP is an approximately 700 residue transmembrane protein with a high affinity Cu^{2+} binding domain between residues 123 and 189 that may be significant in the trafficking of that ion and may play some part in redox deregulation in neuropathology. The amyloid plaques associated with AD largely consist of fibrils arising from the β-strand forms of the N-terminal residues 1–40 or 1–42 derived from proteolytic cleavage of APP. Initially it was believed that Cu^{2+} and/or Zn^{2+} mediated aggregation of Aβ was the basis of its toxicity to neuronal cell cultures and hence its role in AD pathology; there is a better correlation, however, between the level of soluble Aβ oligomers and AD severity than with the number of neuritic plaques containing aggregated Aβ (McLean et al. 1999; Lue et al. 1999).

A major histopathological marker of PD is α-Sn, a 140 residue natively unfolded protein that is the major constituent of Lewy bodies found in the *substantia nigra* of PD patients (Bayer et al. 1999). α-Sn is implicated in conditions such as dementia with Lewy bodies, the Lewy body variant of AD and some less common conditions associated with iron accumulation in the brain as well as in PD. However, the specific mechanism by which α-Sn contributes to PD and other diseases is not clear; physiologically it appears to be involved in modulating synaptic plasticity, neurotransmitter release, presynaptic vesicle pool size and vesicle recycling. Cu^{2+} has been proposed to have a key role in the pathological misfolding and aggregation of α-Sn, although its direct involvement is subject to some controversy, it being suggested that oxidative modification leading to intermolecular cross-linking could be a sufficient explanation (Brown 2007).

The prion protein (PrP^C or simply PrP) is a plasma membrane glycoprotein found at high levels in the central nervous system of all mammalian and avian species. Its physiological function is uncertain, but the finding that PrP^C binds copper ions with low micromolar affinity, coupled with several other observations, suggested that the protein could be important in copper homeostasis. An infectious protease resistant isoform, PrP^{Sc}, is held responsible for fatal transmissible neurodegenerative diseases such as scrapie in sheep, bovine spongiform encephalopathy (BSE, commonly known as mad cow disease) in cattle and variant and sporadic Creutzfeldt-Jacob disease (CJD) in humans. An isoform of PrP^C was also responsible for Kuru, a fatal disease with an incubation period of nearly 50 years and recorded in the Fore population of Papua New Guinea (Collinge et al. 2006; Gajdusek et al. 1967). The central molecular event in the propagation of infectious prions is the conformational conversion into PrP^{Sc} of the isoform of prion protein PrP^C. While the cause of this conformational change of mammalian cellular PrP is unknown, there is reasonable evidence supporting a key role for Cu^{2+} (Brown and Kozlowski 2004). As with Aβ, Cu^{2+} has been proposed to give rise to a gain of toxic function resulting in neurodegeneration (Wood et al. 1999). It must be understood that while one can carry out biophysical and cell culture studies on model systems, the number of possible Cu^{2+}-binding entities, including even the amino acid head group of phosphatidyl serine, ubiquitous in membranes, is so large that we cannot be clear about the molar ratio of Cu^{2+} in the brain to any of the peptides and proteins under discussion. All we can say is that the transition metal ions are markedly elevated in the pathological brain and that reducing their concentrations may be therapeutic (see review by Bush and Curtain, this issue). Even the Cu^{2+} concentrations in the normal brain ($\sim$70 μM) are at the level detectable by modern spectrometers and these are of the order of magnitude of the metal ion concentrations used in the studies referred to in this review.

Although Fe has been shown to play an important part in the Fenton reaction leading to the formation of cytotoxic concentrations of H_2O_2, there is little evidence for significant Fe binding by Aβ, α-Sn and PrP^c. While binding by Cu^{2+} and Zn^{2+} are both important, only Cu^{2+} is paramagnetic and therefore a candidate for electron paramagnetic resonance (EPR) spectroscopic studies of its role in the normal and diseased brain. Such studies can give information about the number and distribution of the Cu^{2+} ions amongst the metal binding sites, their relative orientation, the distance between them, the nature and orientation of the ligands coordinated to the Cu^{2+} sites and the changes occurring during biochemical reactions. Such information can be used to gain an insight into the electronic structure of the Cu^{2+} site and the role played by this ion in the possible biochemical reactions and protein conformational changes associated with neurological diseases. Aside from studies on intrinsic metal ion binding sites, EPR also has the potential for characterising the free radicals involved in ROS-induced damage either by spin-trapping or direct observation. A related application of EPR is in site-directed spin labeling (SDSL) as a probe of distances between paramagnetic sites and a measure of conformational dynamics in amyloidogenic proteins. Although EPR cannot provide all the answers and the technique has its limitations, the information obtained often cannot be readily obtained by other techniques. For example, NMR gives only indirect information about paramagnetic ion binding sites. X-ray crystallography requires the use of single crystals, which are often difficult to grow and may not represent the true behaviour of the metal binding site in the in vivo situation. EXAFS studies do use solutions but require access to a suitable

synchrotron beam line. There may also be issues of interpretation and with the integrity of the sample in the intense radiation beam. It is therefore important to use a number of complementary techniques if a true picture of the role of metal ions in neurological diseases is to be obtained.

In this review we introduce EPR to the non-specialist reader before discussing some issues relevant to the interpretation of EPR spectra of Cu^{2+} in neurobiological systems. We then review the contributions made by EPR to an understanding of the structures of the copper binding sites and how we may gain insight into the formation of some of the potentially toxic species involved in neurodegeneration. Here, we have focused on the EPR of the Cu^{2+} ion bound to the Aβ peptide, as this system is the most studied and Alzheimer's disease is the most significant neurodegenerative disease.

Introduction to EPR

EPR is sometimes but not necessarily strictly correctly referred to as electron spin resonance (ESR) and is an experimental technique for characterizing the energy levels of a system with unpaired electrons in an externally applied magnetic field. The separation of these energy levels as a function of magnetic field depends on the entity on which an unpaired electron is localized and on the nature and structure of the surroundings. For a single unpaired electron, with spin $S = ½$, the energy levels correspond to the two possible orientations of the spin angular momentum vector with respect to the magnetic field direction. The energies of the two orientations differ by $g\beta B$ where g is the spectroscopic splitting factor (the g-value), β is the Bohr magneton and B is the applied magnetic field. For a free electron, $g = 2.0023$. Electron resonance is achieved when this energy difference equals the photon energy $h\nu$ of an oscillating electromagnetic radiation field of frequency ν and where h is Planck's constant. Thus the resonance condition is

$$h\nu = g\beta B \tag{1}$$

If the magnetic component of the oscillating field is directed perpendicular to the applied magnetic field, magnetic dipole transitions are induced in which the magnetic spin quantum number M changes by ± 1. Electrons in the lower state, with $M = -½$, can then absorb energy from the oscillating radiation and be promoted to the higher energy state where $M = +½$. In thermal equilibrium there are fewer electrons in the $M = +½$ state than in the $-½$ state and the ratio of the populations is given by the Boltzmann equation

$$N_+/N_- = \exp -(g\beta B/kT) \tag{2}$$

where k is Boltzmann's constant and T is the absolute temperature. Thus although the probabilities of stimulated emission and absorption are equal, the population difference means that at the resonance condition there will be a net absorption of energy from the oscillating radiation field. The population difference is maintained because the electrons in the $M = +½$ state can lose energy and return to the $M = -½$ state by radiationless relaxation processes, either via interaction with the thermal motions of the system (spin-lattice relaxation) or through spin-spin relaxation due to interaction with other electron (most importantly) or nuclear spins.

Most EPR experiments are carried out in the Continuous Wave (CW) mode with a constant power level for the fixed frequency oscillating radiation and the external magnetic field being swept through the resonance absorption line. The most common radiation frequency is around 9 GHz, so that the magnetic field required for resonance when $g \sim 2$ is around 0.33 T or 3,300 G. Phase sensitive detection is usually used for reasons of sensitivity so that the spectrometer output is displayed as the first derivative of the absorption. More details on the general principles of EPR and the operation of EPR spectrometers are given in texts such as Abragam and Bleaney (1970), Pilbrow (1990) and Weil et al. (1994).

Interpretation of the EPR spectrum of Cu^{2+}: the spin Hamiltonian

The ground state of the Cu^{2+} ion has a $3d^9$ outer electron configuration. The Cu^{2+} complexes encountered in neurobiology are four, five or six-coordinated, with four ligand atoms located in an approximately square planar arrangement around the Cu^{2+} ion. The other coordinating ligands lie along the symmetry axis perpendicular to this plane. This gives a square pyramidal or elongated tetragonal coordination geometry and an axially symmetric environment with the unpaired electron in the $d(x^2 - y^2)$ orbital. The EPR spectrum is conveniently described by a spin Hamiltonian, an operator whose terms involve the electron and nuclear spin vectors and the interaction matrices and tensors. For the axially symmetric Cu^{2+} systems discussed here the spin Hamiltonian is

$$H = \beta\{g_{||}(S_zB_z) + g_\perp(B_xS_x + B_yS_y)\} + A_{||}S_zI_z + A_\perp(S_xI_x + S_yI_y) + H_{\mathrm{shf}} \tag{3}$$

where S_x, S_y and S_z represent the components of the electron spin angular momentum vector along the orthogonal x,

y and z directions, I_x, I_y and I_z similarly for the components of the Cu nuclear angular momentum vector, B_x, B_y and B_z the components of the external magnetic field and the subscripts ∥ and ⊥ denote the components of the g and A interaction matrices parallel and perpendicular to the symmetry axis, taken to be along the z direction. The terms in g, S and B represent the electron Zeeman interaction, where the deviation of the components of the g matrix from the free electron spin value of 2.0023 arise from the admixture of orbital and spin angular momenta. The terms in S, A and I represent the nuclear hyperfine interaction term, arising from the interaction of the electron with the nucleus of the paramagnetic centre. Both the isotopes ^{63}Cu (69.1% abundant) and ^{65}Cu (30.9% abundant) have a nuclear spin $I = 3/2$. Since the allowed $\Delta M = \pm 1$ electron spin transitions take place between pairs of states having the same value of the nuclear spin quantum number m, i.e. $\Delta m = 0$, each electron resonance absorption line will be split into four components for each isotope. The less abundant ^{65}Cu isotope (30.9%) has a nuclear magnetic moment 7% larger, giving a correspondingly larger hyperfine splitting. The hyperfine splitting, being an interaction energy, should be quoted in energy-related units such as cm^{-1} or MHz, rather than in field-related units such as Gauss or Tesla, where $A(\text{Gauss}) \times (0.46686\ g) = A(10^{-4}\ cm^{-1})$.

H_{shf} is the superhyperfine interaction Hamiltonian and represents the interaction of the unpaired electron with the ligand nuclei. The superhyperfine interaction terms have similar form to the hyperfine terms but their principal axes may not coincide with those of g and A.

Terms representing the nuclear quadrupole and nuclear Zeeman interactions are sometimes neglected in the analysis of the CW EPR spectra of Cu^{2+} in neurobiological systems although they are central to the analysis of the ESEEM spectra obtained by pulsed EPR. In cases of interacting Cu^{2+} centres the complete spin Hamiltonian must include the electronic Zeeman and nuclear hyperfine interactions for *each paramagnetic centre* as well as terms of the form $S_i.\boldsymbol{D}.S_j$ where $\boldsymbol{D}$ is a tensor representing the interaction between paramagnetic centres.

The energy levels are obtained from the application of the spin Hamiltonian to the wave functions of the system. Further manipulation either by algebraic means or numerical computation is then used to determine the fields at which the resonances occur. For the axially symmetric monomeric Cu^{2+} systems most commonly encountered in metallo-neurobiology, the resonance field is given to second order in perturbation theory, neglecting superhyperfine, quadrupole and nuclear Zeeman interactions, by

$$B = B_0 - Am/g\beta - (A_{||}^2 + A^2)(A_{\perp}^2/4A^2G)(I(I+1) - m^2) - [\{(A_{||}^2 - A_{\perp}^2)^2/8A^2G\}(g_{||}g_{\perp}/g^2)^2 \sin^2 2\theta]m^2 \quad (4)$$

where $B_0 = h\nu/g\beta$, $g^2 = g_{||}^2\cos^2\theta + g_{\perp}^2\sin^2\theta$, $g^2A^2 = g_{||}^2A_{||}^2\cos^2\theta + g_{\perp}^2A_{\perp}^2 \sin^2\theta$, $G = g\beta B_0$ and θ is the angle between the symmetry axis of the complex and the direction of the applied magnetic field. Consideration of this equation leads directly to the interpretation of the EPR spectrum of a polycrystalline powder or frozen solution if we consider the Cu^{2+} complexes to be randomly oriented at the centre of a sphere and have their symmetry axes intersecting with the sphere at all points on its surface. Since the number of complexes whose symmetry axes lie between the angles θ and $\theta + d\theta$ is given by $N(\theta)d\theta = \frac{1}{2}\sin\theta d\theta$, the probability $N(B)$ of a spin system having a resonant field between B and $B + dB$ is proportional to $\frac{1}{2}\sin\theta/(dB/d\theta)$ (see e.g. Weil et al. 1994, p. 96). This implies that $N(\theta)$ is largest when $dB/d\theta$ is small, which occurs in the simplest cases when θ is 0° or 90°, i.e. the direction of the magnetic field is along the symmetry axis or in the plane perpendicular to it. These considerations lead to an explanation of the commonly observed spectra of Cu^{2+}, where the most prominent regions of the spectrum are those associated with $g_{\perp}$ and the less prominent with $g_{||}$. Typical Cu^{2+} systems have $g_{||}$ ranging from ~2.2 to 2.4 and $g_{\perp} \sim 2.05$. Since $A_{||} \gg A_{\perp}$ (typically $A_{||} \sim 150$–$200 \times 10^{-4}\ cm^{-1}$, $A_{\perp} \sim 10 \times 10^{-4}\ cm^{-1}$) the hyperfine structure in the parallel direction is resolved into up to four peaks whereas that in the perpendicular direction is usually not resolved.

Spectrum simulations

Although it is convenient to estimate spin Hamiltonian parameters from an inspection of the experimental spectra, such practices can give misleading results. The existence of second order terms, off-axis extrema, line broadening phenomena and the possibility that the obvious spectrum is superimposed on resonances due to other species all require that simulations be performed to fully characterise the spectrum. The principles of computer simulation of EPR spectra have been discussed e.g. Pilbrow (1990) and EPR spectrum simulation programs such as those in the SOPHE® suite (Hanson et al. 2004) are available commercially or as freeware. To quote Pilbrow (1990, p. 259) "…it is not necessarily correct simply to read hyperfine splittings from the 'absorption'-like 'parallel' peaks until one is sure about the origins of the lineshape. Nowadays we must argue for high level simulations for proper quantitative evaluation of EPR spectra."

Identification of Cu^{2+} sites

The Peisach–Blumberg plots

A qualitative picture of the Cu^{2+} binding site may be obtained through the empirical scheme of Peisach and Blumberg (1974). This correlates $g_{\|}$ and $A_{\|}$ for a number of arrangements of known ligands as shown in Fig. 1. Although there is a theoretical justification for this procedure in crystal and ligand field theories (Bleaney et al. 1955; Maki and McGarvey 1958), the plots are often applied without consideration of their limitations. Firstly, the regions of the plots for different coordination modes show considerable overlap, as shown in Fig. 1. Secondly distortions from square planar towards tetrahedral geometry have the effect of shifting $g_{\|}$ and $A_{\|}$ in opposite directions (Yokoi and Addison 1977), thus appearing to change the coordination mode. The inferences of coordination drawn from the plots should therefore be used as a guide only. It is worth noting that the values of $A_{\|}$ in Peisach and Blumberg (1974) are given in mK (millikaisers, where 1 mK = 0.001 cm^{-1}) and are in effect for ^{63}Cu which has a 7% smaller hyperfine interaction than ^{65}Cu.

Superhyperfine structure

Where the atoms binding to the Cu^{2+} ions have nuclear magnetic moments, the electron resonance lines may exhibit superhyperfine structure due to the interaction of these nuclear magnetic moments with the electron magnetic moment. The most common superhyperfine interactions observed in neurobiological EPR are those due to nitrogen nuclei. The ^{14}N nucleus has a nuclear spin $I = 1$ and the electron resonance line is then split into three components of equal intensity. If there are P equivalent nuclei, $P(2I) + 1$ components are possible with relative intensities given through Pascal's triangle. Thus, the number and relative intensities of the superhyperfine resonance lines can be used to determine the coordination to the Cu^{2+} ion. At around 9 GHz it is often possible to observe ^{14}N hyperfine splittings in the $g_{\perp}$ region of the spectrum as a series of partially resolved resonances separated by $\sim$14 G. In some circumstances, *g–A* strain effects lead to better resolution of superhyperfine interaction patterns being obtained from the parallel peaks of the Cu^{2+} hyperfine resonances in the frozen solution spectrum when lower microwave frequencies, e.g. $\sim$4 GHz, are used. As a guide, and assuming that the superhyperfine interactions are isotropic *and those from different nuclei are magnetically equivalent*, coupling to two ^{14}N ligands gives five lines with relative intensities in the ratios 1:2:3:2:1. Similarly, for three ^{14}N ligands, seven lines are expected with intensity ratios 1:3:6:7:6:3:1. For four ^{14}N ligands the spectrum should exhibit nine lines with intensities in the ratio 1:4:10:16:19:16:10:4:1. A simplification of the ^{14}N superhyperfine interaction pattern is achieved if ^{15}N is substituted for ^{14}N either globally or for specific sites in known residues. ^{15}N has a nuclear spin $I = ½$ and a slightly larger nuclear magnetic moment, giving both fewer and more widely spaced superhyperfine resonances. For a single ^{15}N nucleus, two lines of equal intensity are observed; for two ^{15}N nuclei, three lines with relative intensities 1:2:1, for three ^{15}N nuclei four lines with intensities 1:3:3:1 and for four ^{15}N nuclei, we expect five lines with intensities 1:4:6:4:1. Despite the apparent simplicity, the number of peaks in a superhyperfine pattern can be misleading if the interaction is anisotropic or the ligands are not magnetically equivalent. Additional confusion can occur due to *g–A* strain broadening effects and if $A_{\perp}$ has a similar magnitude to the ligand superhyperfine interaction. Spectral simulations are therefore essential for the unambiguous determination of the number of contributing nuclei.

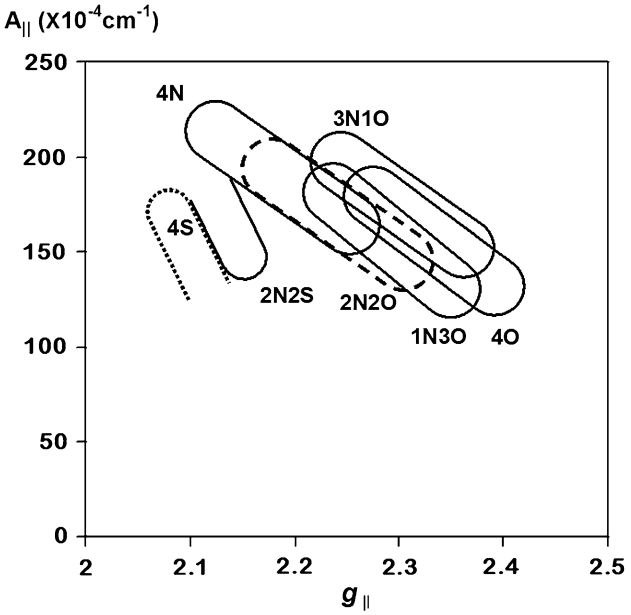

Fig. 1 Plot of $A_{\|}$ versus $g_{\|}$ with the range of Cu^{2+} coordinations found in the literature, showing the extent of overlap between these. Originally devised Peisach and Blumberg (1974), the present plot was adapted from Pilbrow (1990). Note, in the original plots of Peisach and Blumberg (1974) the formal charge dependence within each region ranged from −2 at the *upper left hand corner* to +2 at the *lower right hand corner*

Determination of coordination environment using pulsed EPR

High-resolution EPR spectroscopies such as ESEEM and ENDOR can sometimes be usefully applied to the study of Cu^{2+} systems where conventional CW EPR does not resolve the superhyperfine interactions (Deligiannakis et al. 2000). ENDOR techniques, which can be both CW and

nowadays, more usefully, pulsed are best applied to strongly coupled nuclei directly coordinated to the paramagnetic centre. ESEEM is most useful where there is weak coupling between the electron spin and the nuclear spins more distant from the paramagnetic centre, such as the distal nitrogen of the imidazole ring of a histidine residue. Thus, CW EPR, detecting the superhyperfine structure from directly coordinated nitrogen ligands, and ESEEM, detecting the more remote nitrogens provide a very powerful combination for characterizing the Cu^{2+} binding site.

Unfortunately, the application and interpretation of ESEEM is not always straightforward for Cu^{2+} systems. Sample temperatures below 20 K are usually required and determining the optimum conditions of pulse width and power and pulse sequence can be time consuming. The analysis of the spectrometer output requires Fourier transform techniques and is also prone to the generation of artefacts. When the modulation is provided by a single distal nitrogen from imidazole, a characteristic "three narrow plus a broad line" spectrum is observed. If two or more nitrogens are involved, combination peaks are observed between the narrow and broad peaks. The number and relative intensity of these combination peaks depends on the number of nitrogens involved, as shown by McCracken et al. (1988) for some simple model complexes. ESEEM experiments employing two dimensional correlation pulse sequences, such as HYSCORE (see e.g. Van Doorslaer et al. 2001) are sometimes useful in confirming the number and type of nuclei present and their distance and orientation relative to the paramagnetic centre. Unfortunately, the determination of the number of histidine residues from these experiments may not be straightforward, as the distal nitrogens may not be equivalent and amide nitrogens at similar distances may contribute to the spectrum.

Spectral resolution, line broadening and broad lines in Cu^{2+} EPR spectra

Line broadening due to spin relaxation effects

Line broadening and the consequent loss of resolution of superhyperfine and even hyperfine splittings can occur if the spin relaxation time is either very short or very long. If the spin relaxation time is much shorter than $\sim 10^{-10}$ s, lifetime broadening will occur as a result of the uncertainty principle. Spin-lattice relaxation times are strongly temperature dependent and in some Cu^{2+} systems broadening may occur at temperatures higher than about 150 K. This necessitates the use of cryogenic techniques to minimize line broadening and maximize spectral resolution. If the spin-lattice relaxation times are very long, as often occurs at temperatures in the liquid helium range, line broadening and loss of spectral resolution can be observed due to microwave power saturation effects. These are readily observed if the Cu^{2+} ions are magnetically isolated and if the microwave power levels are elevated in order to improve the spectrometer sensitivity. In order to minimise saturation effects, the microwave power must be reduced, often to the nW level, at liquid helium temperatures. Further consequences of long relaxation times and high power levels may be the observation of absorption-like spectra in the derivative presentation as a result of adiabatic rapid passage effects (see e.g. Abragam and Bleaney 1970).

Line broadening due to *g*–*A* strain

The resolution of hyperfine and superhyperfine structure in the frozen solution spectra of many Cu^{2+} complexes has been observed to depend on the microwave frequency and the nuclear spin magnetic quantum number, m. These phenomena were first given a quantitative explanation by Froncisz and Hyde (1980). The effects arise because of the correlations between $g_{\|}$ and $A_{\|}$ (noted above in connection with the PB plots) and the statistical distribution of these parameters as a result of random strains at the Cu^{2+} binding site. These strains are readily induced when simple complexes are frozen but also commonly occur in the complex neurobiological systems as a result of variations in peptide conformation. They must be properly accounted for when attempting to determine $g_{\|}$, $A_{\|}$ and the number of coordinating nitrogen ligands. It is therefore essential that computer simulation programs include linewidth terms providing for *g*–*A* strain effects.

Line broadening and broad lines due to interactions between Cu^{2+} ions

Line broadening effects and broad lines arising from dipolar and exchange interactions between Cu^{2+} ions must be distinguished from the effects of line broadening mechanisms such as those due to spin relaxation or strain broadening as described earlier.

Exchange interactions are due to the overlap of electron densities between two or more centres via a bonding pathway. Their magnitude may range from ~ 500 cm^{-1} to less than 1 cm^{-1} (Hodgson 1975) and can therefore significantly affect the EPR spectrum. Dipolar interactions are due to the "through space" interaction of the magnetic moments of the Cu^{2+} ions and will always be present if two or more Cu^{2+} ions are close together. They do not require a bonding pathway. Their magnitude depends on $1/r^3$, where

r is the distance between the ions. A useful guide is that their magnitude is around 0.1 cm^{-1} (rather larger than the hyperfine interaction) for a separation of 3 Å, around 0.01 cm^{-1} (approximately the magnitude of the hyperfine interaction) at a separation of 6 Å and around 0.001 cm^{-1} or approximately the magnitude of common N ligand superhyperfine interactions at a distance of 12 Å. We can see from the above that dipolar interactions will have a significant influence on the EPR spectrum when the ions are closer than around 10 Å and may still contribute to line broadening at rather greater distances. For a number of Cu^{2+} ions within 10−12 Å of each other but not necessarily in a specific geometrical arrangement, the dipolar interactions result in a broad resonance centred near the average g-value. Such resonances are often narrower than expected due to the presence of weak exchange interactions between the Cu^{2+} ions (Van Vleck 1948; Abragam and Bleaney 1970, p. 527–529).

A special case of relevance to Aβ: EPR spectra due to interacting pairs of Cu^{2+} ions

Smith and Pilbrow (1974) and Bencini and Gatteschi (1990) have provided comprehensive reviews of the EPR spectroscopy of interacting pairs of paramagnetic ions. When two Cu^{2+} ions are within about 10 Å of each other and are magnetically isolated from other paramagnetic centers, the dipolar and exchange interactions result in the coupling of the two electron spins, each with $S = ½$, to give a singlet state (total spin $S = 0$) and a triplet state with total spin $S = 1$. The dipolar interaction splits the singlet state from the triplet state and gives a zero-field splitting of the triplet state. The magnitude of these splittings is dependent on $1/r^3$. Isotropic exchange interactions also split the singlet state from the triplet state but do not give a zero-field splitting of the triplet state. Anisotropic exchange interactions are second order effects and are able to split the levels of the triplet state, but are usually at least an order of magnitude smaller. For most Cu^{2+} systems, the isotropic exchange, of magnitude J, is negative, so that the singlet state is lower in energy. If $kT \ll |J|$, where T is the temperature and k is Boltzmann's constant, only the singlet state is populated and the system has no magnetic moment and appears to be EPR silent. If $J \ll kT$ or the interaction is purely dipolar (i.e. $J = 0$) the spectral intensity of a coupled paramagnetic system follows a $1/T$ dependence, just as an uncoupled system. Thus the observation that the intensity of a particular EPR signal shows a dependence on $1/T$ down to very low temperatures does not exclude the possibility of interactions between Cu^{2+} ions.

When the triplet state is populated, intense EPR signals can be observed due to the "allowed" electron spin transitions between the $M = 0$ and $M = \pm 1$ levels of the triplet, i.e. where $\Delta M = \pm 1$. For Cu^{2+} ions, these will be centered near $g = 2$, with a separation dependent on the zero-field splitting of the triplet state. Less intense resonances due to "forbidden" transitions where $\Delta M = \pm 2$ are also possible and may be observed at approximately half the magnetic field of the allowed transitions, i.e. near $g = 4$. If the coupling is purely dipolar and exchange interactions are small, their intensity may be ~1/500th or less than that of the allowed transitions for an internuclear distance around 6 Å. However, their observation, usually requiring sensitive EPR spectrometers operating at very high system gains, is diagnostic for the presence of Cu^{2+} ions in close proximity, irrespective of the resonances at $g \sim 2$ which may be dominated by the spectra of magnetically isolated Cu^{2+} ions.

Magnitudes of zero-field splittings are readily determined by EPR, so that the distance between the Cu^{2+} ions can be estimated provided that the zero-field splitting of the triplet state is due to dipolar interactions alone. This is generally assumed to be the case if $|J| < 30$ cm^{-1}. The observation of the $g \sim 4$ resonances at 4 K implies that $|J|$ is less than ~10 cm^{-1} and second order exchange effects can be neglected. Since the appearance of the resonances is affected by the relative orientations of the g and A matrices of the ions, as well as by the distance between them, computer simulation of both $\Delta M = \pm 1$ and $\Delta M = \pm 2$ resonances is essential and can also give much biologically relevant detail.

The use of site-directed spin labeling (SDSL) to probe distances and measure conformational dynamics in amyloidogenic proteins

SDSL relies on the covalent attachment of a nitroxide sidechain to the sulfhydryl groups of cysteine residues that have been introduced into the protein by site-directed mutagenesis (Berliner 1983). It is mentioned here because it could provide complementary data about structures where interactions between Cu^{2+} ions occur. SDSL can be used for the determination of structure and conformational dynamics in both soluble monomeric, oligomeric and membrane proteins because spectral shapes and line width are dependent on the local motion in the label's environment and the distance between labels. Typically, spin–spin interactions between nitroxide labels in proteins are dominated by dipolar effects that result in spectrum broadening, providing distance information in the range of ~8–25 Å. Using only picomoles of each labeled protein, spectrum analysis can be used to determine the three-dimensional structure of a protein at the level of the backbone fold, with a real-time resolution in the millisecond range. For

example, with amyloidogenic proteins, if a single label is present on each protein molecule, EPR spectra will give information on intermolecular contact sites and packing of individual protein monomers in the fibril. If paramagnetic ions are present, interactions between the label and these can provide further information about the metal binding sites in the protein. The technique has not been used to its full potential in the few studies on these neuroproteins, probably because this requires sophisticated EPR spectrometers, such as Fourier transform instruments capable of pulsed double electron–electron resonance experiments as used, for example, in an SDSL study of the structure of the inhibitory region of tropinin (Brown et al. 2002).

The same caveat, the need for careful and accurate simulation, applies to the analysis of spin-label spectra, as for metal ion spectra. Another caveat is that, in common with all spin label techniques, SDSL involves the addition of a bulky nitroxide group to a cysteine residue that may not have been in that position in the native protein, thereby altering the latter's conformation. Complementary techniques include photo-induced cross-linking and multiple quantum ^{13}C solid state NMR. Neither can give the dynamic information yielded by SDSL, but can show relationships between residues on adjacent chains.

EPR of the copper binding domain of the amyloid precursor protein

A study of the Cu^{2+} site of CuBD (Barnham et al. 2003b), indicated, through broadening of some of the resonances in the NMR spectrum, that the relevant binding site involved the residues His-147, His-151, Tyr-168 and Met-170. The EPR spectrum of 0.3 mM $^{65}Cu^{2+}$ added as $Cu^{2+}(gly)_2$ to 0.5 mM CuBD (133–189) in 20 mM pH 6.9 PBS buffer exhibited orthorhombic symmetry with *g*- and *A* values consistent with a distortion away from square planar to a more tetrahedral arrangement. The principal *g* and *A* values were correlated with the region in the PB scheme corresponding to 2NSO coordination, consistent with the NMR data. We note that the broadening or even the disappearance of NMR resonances can be induced by the presence of paramagnetic centres as far away as 10 Å.

A series of fragments of CuBD, namely APP (145–155) and APP (145–157) have been studied by Valensin et al. (2004). From the combination of NMR, UV–Vis, CD and EPR spectroscopies and potentiometric measurements, these authors concluded that the Cu^{2+} binding site involved coordination to an imidazole nitrogen of each of His-147, His-149 and His-151 and to the amide nitrogens of Leu-148 and His-149. Their overall conclusion, of a Cu^{2+} binding site involving five nitrogens, is not in accord with the findings of the studies of the longer constructs referred to in this section and highlights the dangers of basing an understanding of the behaviour of full length sequences on that of short fragments.

The high resolution picture of the Cu binding site of the CuBD given by the recent X-ray crystallographic study of Kong et al. (2007) showed that the Cu^{2+} ion was bound to two N atoms (His-147 and His-151), the hydroxyl oxygen of Tyr-168, an "equatorial" water about 1.4 Å above the plane of the amino acid ligands and an axial water about 3.0 Å above the plane. The Cu^{2+} atom is located about 0.6 Å above the plane towards the axial water and is in a distorted square pyramidal configuration. The X-ray crystallographic evidence rules out direct coordination to Met-170. This description of the binding site is supported by solution EXAFS and the EPR of frozen solutions. The EPR spectrum of 2 mM CuBD (133–189) in 20 mM 2-(N-morpholino) ethanesuphonic acid buffer at pH 6.8, to which 1.2 mM $CuCl_2$ was added prior to freezing to 120 K, exhibited axial symmetry and clearly resolved peaks due to ^{14}N superhyperfine interactions in the perpendicular region of the spectrum. Although the initial inspection indicated the possibility of 3N coordination, simulations including *g*–A strain broadening clearly showed coordination by two and only two equivalent N ligands. This illustrates the need for careful simulations taking into account line broadening mechanisms and other effects leading to spectral distortions.

The differences between the EPR spectra of Barnham et al. (2003b) and Kong et al. (2007), illustrate several of the difficulties encountered in EPR studies of metallo-neurobiological systems. Firstly, the values of $g_{\|}$ and $A_{\|}$ of Kong et al. (2007) when applied to the PB plots are consistent with 2N2O coordination, although they also fall into the region for 3N1O. This serves to illustrate that these plots, while useful in the absence of more specific information, are not definitive. This caution is further illustrated by the interpretation of the spectrum by Barnham et al. (2003b) as being due to coordination by 2N1S1O but the parameters are also consistent with 2N2O coordination, albeit in a site with a distortion more towards tetrahedral.

Secondly since both CuBD preparations originated from the same construct, the differences in EPR spectra must be due to handling procedures. Possibilities include time factors, the concentrations of both peptide and copper in solution, the use of $Cu^{2+}(gly)_2$ rather than $CuCl_2$ as the copper carrier and what may be the most critical, the use of PBS buffer by Barnham et al. (2003b) and MES buffer by Kong et al. (2007). This implies a significant role for the buffer in the configuration of the metal binding site and quite possibly, the conformation of the protein.

Nevertheless, this study was the first where a protein of neurological interest was the subjected to a combination of structural determination techniques giving a clearer picture

of its metal ion binding site than would be possible with a single technique alone (see review by Parker et al. in this issue).

The EPR of Cu^{2+}-Aβ

The assembly of the amyloid plaques characteristic of AD proceeds through various stages of aggregation from soluble monomeric species through soluble aggregates of increasing complexity, some of which may be dimeric, to essentially insoluble spherical oligomers approximately 100–200 Å in size (see e.g. Miura et al. 2000; Antzutkin 2004; Smith et al. 2007). The equilibrium between these species appears to be driven in the first instance by the Cu/peptide ratio but there is a dependence on yet unquantified conditions such as overall peptide concentration, buffer, salt concentration and temperature and time after addition of Cu^{2+}. EPR signals corresponding to monomeric Cu^{2+}Aβ at Cu^{2+}/Aβ molar ratios below $\sim$0.5, a dimeric $(Cu^{2+}/A\beta)_2$ species at Cu^{2+}/Aβ molar ratios above about 0.5 and a broad resonance appearing at Cu^{2+}/Aβ ratios greater than $\sim$1.0 and attributed to a number of Cu^{2+} ions $\sim$10 Å apart have all been identified and are consistent with different states of aggregation (Curtain et al. 2001, 2003; Smith et al. 2006). These EPR measurements used Aβ of lengths 1–16, 1–28, 1–40 and 1–42 in PBS buffer over the pH range 5.0–8.0, though mainly in the physiologically relevant range of 6.9–7.4.

The binding site of Cu^{2+} to Aβ at low Cu^{2+}/Aβ molar ratios

At low Cu^{2+}/Aβ molar ratios up to about 0.5, the spectra of Cu^{2+} bound to unmodified Aβ at physiological pH are characteristic of magnetically isolated (monomeric) Cu^{2+} in an axially symmetric environment with square-planar, square-pyramidal or elongated tetragonal geometry. The dominant coordination mode near physiological pH has spin Hamiltonian parameters typically in the ranges $g_{\|} \sim$ 2.26–2.27 and $A_{\|} \sim$ 160–190 $\times$ 10^{-4} cm^{-1} (where $A_{\|}$ splittings refer to the ^{63}Cu isotope). These values are consistent with 3N1O coordination on the PB plots, although other combinations such as 2N2O and 4N are also possible. They are also consistent with those found by other authors (Huang et al. 1999; Antzutkin 2004; Syme et al. 2004: Karr et al. 2004). The spectrum broadens as the Cu^{2+}/Aβ molar ratio approaches 0.5, presumably due to dipolar interactions with nearby Cu^{2+} ions.

As regards the binding site, Huang et al. (1999) observed superhyperfine structure indicative of Cu^{2+} bound to at least three nitrogen ligands, but this result has not been replicated by other authors. NMR measurements (Curtain et al. 2001) showed that the C2H and C4H peaks assigned to the histidine residues H6, H13 and H14 disappeared on addition of Cu^{2+} to solutions of Aβ 1–28 and Aβ 1–40 in PBS at pH 6.9, thus suggesting that these three His residues provide the three nitrogen ligands of the binding site. Most later studies showed a consensus on the involvement of the three histidines in the principal Cu^{2+} binding site of Aβ (see Syme et al. 2004; Karr et al. 2004, 2005; Guilloreau et al. 2006), but Kowalik-Jankowska et al. (2003) have put forward evidence for an alternative coordination. On the other hand, the identity of the fourth ligand is as yet unresolved.

The NMR measurements of (Curtain et al. 2001) suggested that the fourth ligand is oxygen from the tyrosine residue Y10, a view supported by the observation that the substitution Y10A gave different spin Hamiltonian parameters to the unmodified peptide (Barnham et al. 2004). Support for this model is provided by the EXAFS measurements of Stellato et al. (2006), who propose coordination to the Cu^{2+} site by three histidines (presumed to be H6, H13 and H14), a tyrosine residue (presumably Y10) and an OH- ligand in a pentacoordinated structure. However both Syme et al. (2004) and Karr et al (2005) have suggested the involvement of the N-terminal amide nitrogen in the Cu^{2+} binding site. As regards the possible oxygen ligand, Karr et al. (2005) found that the Y10F modified peptide had the same spin Hamiltonian parameters as the full-length peptides, thus suggesting that the Y10 residue is not the source of the O ligand. Isotopic labelling experiments showed that water was not the O-atom donor in the Y10F mutant (Karr et al. 2005). Other possible oxygen ligands may be the carboxylate groups of D1, E3, D7 or E11, although Karr and Szalai (2007) have ruled out the latter three. Oxidised Met-35 does not appear to be the source of the oxygen ligand, even though this residue appears to be pivotal to Aβ toxicity and membrane binding and has been implicated as an electron donor in ROS production (Barnham 2003a; Ciccotosto et al. 2004).

Given the uncertainties resulting from interpretations of the PB plots, the only concrete EPR evidence for the coordination to the binding site is the observation, so far apparently not replicated, of superhyperfine structure due to "at least three nitrogen atoms" (Huang et al. 1999). In the absence of definitive EPR evidence such as superhyperfine structure and because of the uncertainties in the interpretation of the PB plots, deductions based on changes in the spin Hamiltonian parameters of Cu^{2+} bound to some of the modified Aβ peptides and Aβ peptide fragments can only be regarded as indicative (see e.g. Kowalik-Jankowska et al. 2002; Karr et al. 2005: Karr and Szalai 2007; Dong et al. 2007). Although the EXAFS results of Stellato et al. (2006) are consistent with the model proposed by

Curtain et al. (2001, 2003), the possibility still remains of binding sites with two or more combinations of coordinated residues (see e.g. Guilloreau et al. 2006). This raises the possibility of different peptide conformations and thence to different arrangements of the peptide chains on aggregation, as has been suggested by Miura et al. (2000).

Cu^{2+}/Aβ molar ratios from 0.5 to 1.0

The development of a broad featureless resonance in the $g \sim 2$ region and a much weaker resonance at $g \sim 4$ has been observed for each of Aβ 1–16, Aβ 1–28, Aβ 1–40 and Aβ 1–42 at Cu^{2+}/Aβ molar ratios above about 0.5 and over the pH range 5.5–7.5 in PBS (Curtain et al. 2001, 2003; Smith et al. 2006). The $g \sim 2$ resonance was quite distinct from the monomeric spectrum and was attributed to the $\Delta M = 1$ transitions within a triplet state arising as a result of exchange and/or dipolar coupling between two Cu^{2+} ions about 6 Å apart. The $g \sim 4$ resonance was only observed at very high spectrometer gains and was attributed to the forbidden, or $\Delta M = 2$ transitions within the triplet state. The observation of both these resonances at 2.5 K showed that the zero-field splitting of the triplet state is due to dipolar interactions alone. The model of the dimeric species proposed by Curtain et al. (2001, 2003) and Smith et al. (2006) is of one Cu^{2+} ion bound to the His-13 and His-14 residues on each of two peptides, with the Cu^{2+} ions being bridged through the imidazole nitrogens of one of the His-6 residues. Spectrum simulations on the basis of purely dipolar coupling gave a distance between the Cu^{2+} ions of 6.2 ± 0.2 Å and a spatial arrangement that was regarded as consistent with the formation of a histidine bridge (Smith et al. 2006).

The histidine bridge model was supported by the inability to observe the $g \sim 2$ and $g \sim 4$ resonances for Aβ 40 and Aβ 42 at Cu^{2+}/Aβ ratios approaching 1.0 when the histidine residues 6, 13 and 14 were substituted by histidines methylated at either the π- or τ- nitrogen of the imidazole ring (Tickler et al. 2005; Smith et al. 2006). Although the histidine bridges found in $Cu^{2+}Cu^{2+}$SOD and some model complexes have rather larger exchange interactions than found here (Ohtsu et al. 2000), such factors as the distance between the Cu^{2+} ions and bond angles can lead to much smaller exchange (Haddad and Hendrickson 1978). The intensity of the resonances at $g \sim 4$ relative to those at $g \sim 2$ is also dependent on the magnitude of the exchange interaction. Thus the much lesser intensity of the $g \sim 4$ resonances relative to those at $g \sim 2$ in the present case is consistent with essentially pure dipolar coupling and only very weak exchange. We should also remember that a histidine bridge is not necessary for dipolar coupling, which is a through space and not a through bond interaction.

In contrast to these observations, neither Karr et al. (2004) nor Syme et al. (2004) could find EPR evidence for interactions between Cu^{2+} sites. However, the similarity of the spectra in Fig. 3 of Syme et al. (2004) for Cu^{2+}/Aβ ratios of 2.0 and greater to those reported by Curtain et al. (2001, 2003) and Smith et al. (2006) suggests the presence of dimeric species. Neither Karr et al. (2004) nor Syme et al. (2004) report spectrum simulations, without which it is impossible to be confident that the monomeric spectrum is not superimposed on a background due to the dimeric spectrum. It should also be noted that a dependence of the spectral intensity on $1/T$ down to very low temperatures is not a definitive indicator of the absence of interactions between Cu^{2+} ions. Further, Cu^{2+} concentrations of ~50 μM, rather lower than that used by Smith et al. (2006), may have prevented the observation of the $g \sim 4$ resonances that are the definitive indicators of the presence of dimeric species. The inability to observe the $g \sim 4$ resonances, even under spectrometer settings of optimum signal/noise and maximum spectrometer gain, does not mean that such species do not exist- only that they may be at too low a concentration to be observed.

In summary, the appearance of broad $g \sim 2$ resonances, and $g \sim 4$ resonances, when conditions enable their detection, is diagnostic of a particular state of association of Aβ peptides, regardless of whether this is due to histidine bridging or to an increase in the hydrophobicity of the N-terminus arising from the deprotonation of the histidines by Cu^{2+} ligation. With regard to the latter possibility, it is significant that the broad $g \sim 2$ resonances are found in spectra of Aβ-Cu^{2+} in phosphate buffered physiological saline and that NaCl has been found to be a significant promoter of Aβ association (Huang et al. 1997; Narayanan and Reif 2005), arguing for a role for electrostatic shielding in Aβ association.

EPR of Cu^{2+}/Aβ aggregates: Cu^{2+}/Aβ molar ratios of 1.0 or greater

At Cu^{2+}/Aβ molar ratios around 1.0 or greater, the spectrum in the $g \sim 2$ region showed evidence of another broad resonance with a peak at a slightly lower field (Smith et al. 2006) and a g-value ~2.14. The resonance is attributed to the interaction of a number of Cu^{2+} ions about 10 Å apart and in a structurally less ordered aggregate. The dipolar interactions are modulated by weak exchange, giving an exchange-narrowed resonance with a g-value close to the average of the monomeric g-values. This is consistent with the development of larger aggregates such as the small insoluble spherical oligomers 100–200 Å in size reported by Smith et al. (2007). Although they were unable to observe EPR signals due to interactions between

Cu^{2+} ions, the findings of Karr et al. (2004) that Cu^{2+} binds to fibrils initially assembled without Cu^{2+} in the same coordination environment as in fibrils assembled with Cu^{2+} and that the ligand donor set does not change during the organization of Aβ monomers into fibrils are not inconsistent with the above. The multiple quantum NMR results of Antzutkin et al. (2000) indicating a parallel organization of the polypeptide chains within the amyloid fibrils are also consistent with the EPR results.

Correlation with other structural studies

Since Aβ is a small protein, it cannot be crystallised, except as part of a larger complex. Here, complementary X-ray diffraction and X-ray absorption techniques can be employed to obtain accurate structural information. Streltsov in this issue reviews progress in this area.

Physiological correlations with the EPR spectroscopic results

Smith et al. (2006) conjoined a number of physiologically important observations to the appearance of the $g \sim 4$ resonances. As discussed above, the resonances at $g \sim 2$ and $g \sim 4$ diagnostic for Cu^{2+} dimeric species could not be observed on methylation of either the τ- or π-nitrogen of the imidazole side chains of the histidine residues. In comparison with the wild type Aβ-Cu^{2+} complex, His methylation also attenuated toxicity to cultured primary cortical neurons, diminished the formation of dityrosine adducts by Aβ-Cu^{2+} incubated in the presence of H_2O_2 and attenuated lipid peroxidation on incubation with phospholipid vesicles in the presence of ascorbate. Further, toxicity did not correlate with the formation of amyloid, which, contrary to the findings of Karr et al. (2004), was found to occur only at Cu^{2+}/Aβ ratios <1.0. Tickler et al. (2005) had observed the same lack of toxicity for Aβ 1–40 where the histidines had been methylated, indicating that the effect was independent of the changes in hydrophobicity of the peptide at the C-terminus. As well as confirming the lack of amyloid toxicity, the observations of Smith et al. (2006, 2007) point to the possibility that in vivo formation of the toxic species of Aβ would be subject to the availability of exchangeable Cu^{2+}, the diminution of which would reduce cytotoxicity. This is line with the observations that treatment with a relatively weak blood–brain barrier permeable Cu-binding compound (clioquinol) led to significantly more stable general health and body weight parameters in APP2576 transgenic mice, expressing the human amyloid precursor protein (Cherny et al. 2001). This compound also showed promising results in a limited phase II clinical trial (Ritchie et al. 2003) in AD patients.

Alpha-synuclein (α-Sn)

A recent review (Brown 2007) has highlighted some of the controversial issues regarding α-Sn. Among these are whether α-Sn has a physiologically relevant function, whether the binding of Cu^{2+} is biologically relevant and the number and nature of the Cu^{2+} binding sites, as well as their role in fibrillar formation.

Rasia et al. (2005) used a combination of UV–Vis, CD, NMR and EPR spectroscopies to identify two copper binding sites in α-Sn. A frozen solution at 77 K of the 1:1 Cu^{2+} complex of wild type α-Sn at 0.3 mM concentration in buffer at pH 6.5 exhibited an EPR spectrum characteristic of an axially symmetric system. This was of Cu^{2+} in the primary binding site, located in the N terminus involving His-50 and the N-terminal amide nitrogen. These authors obtained a very different spectrum of a Cu^{2+} α-Sn complex in which the His-50 residue had been blocked by reaction with DEPC. This spectrum was presumed to originate from a Cu^{2+} binding site in the C-terminus, having 1/300th the affinity of the primary site. From the PB plots and related literature, Raisa et al. (2005) proposed that the Cu binding site in WT α-Sn at pH 6.5 was 2N2O and in the His-50 blocked α-Sn, the Cu^{2+} was coordinated by four oxygens.

However, the potential for α-Sn to bind Cu^{2+} at up to ten sites has been reported (Paik et al. 1999). Sung et al. (2006) suggest that binding at up to 16 sites is possible. Kowalik-Jankowska et al. (2005) report that the N-terminal fragments of α-Sn can bind Cu^{2+} with coordination modes ranging from 2N to 4N. Sung et al. (2006) also showed that DEPC treatment is not specific to His-50, and can block other Cu^{2+} binding sites. In particular, they argued against the possibility of a coordination mode involving both the N-terminal amine and His-50.

In addition to Brown's (2007) reservations concerning the significance of binding to α-Sn in the light of the relatively weak association constants, there are also concerns about the reliance on the PB plots, given that the *g*-values are capable of assignment to multiple regions.

SDSL has been used to show that monomeric α-synuclein had a highly dynamic structure in solution, while fibrillar aggregates had a distinct domain organization (Der-Sarkissian et al. 2003). The latter consisted of a highly ordered and specifically folded central core region of approximately 70 amino acids, a structurally more heterogeneous N terminus and a completely unfolded C terminus of approximately 40 amino acids. The central core region had a number of features including an in-register parallel structure reminiscent of those observed in the core region of fibrillar Aβ. It was concluded that, although the lengths of the respective core regions differ, fibrils from different amyloid proteins nevertheless seem to be able to take up highly similar, and

possibly conserved, structures. There are no time resolved SDSL studies on α-synuclein oligomerization so the potential for SDSL to contribute to our understanding of the protein's folding dynamics is unknown.

EPR of PrP

The EPR of PrP^C with particular reference to Cu^{2+} PrP^C has been reviewed recently (Drew and Barnham 2007) and will not be detailed here. Papers such as those from Burns et al. (2003) and Van Doorslaer et al. (2001) may be cited as examples of the applications of CW EPR at X and S band microwave frequencies, ENDOR and ESEEM techniques to the unravelling of the structures and locations of the Cu^{2+} binding sites. There remain controversies regarding the relative binding affinities of each of the Cu^{2+} sites, the mode of the octarepeat coordination at intermediate Cu occupancy, the physiological relevance of the results obtained for the shorter PrP fragments and the role of metal ions in promoting the changes from PrP^C to PrP^{Sc}.

There have been three SDSL studies on PrP. The earliest (Lundberg et al. 1997) was a kinetic study of the aggregation and amyloid formation by 113–120 fragment, while later work (Inanami et al. 2005; Watanabe et al. 2006) focussed on the full 23–231 sequence to show that the region containing the fifth Cu^{2+} binding site around His-96 is more flexible than Helix 1 and Helix 2. There is a pH dependent conformational change in the conversion of PrP^c to PrP^{sc} (Watanabe et al. 2006) and this was considered to be reflected in a pH dependence in the mobility of helix 2 as revealed by SDSL. Here, again the surface has been barely scratched and the field is wide open for detailed dynamics and folding energy landscape studies by advanced SDSL and other techniques.

Conclusions

As described in this paper, EPR measurements have given much detail about the structure and modus operandi of metal binding sites in neurobiological systems. As we have seen, there are still many issues remaining unresolved. To obtain satisfactory answers to these questions will require the use of high-resolution EPR measurements and analysis in conjunction with other structural and biophysical measurements. Key factors in all these measurements are the needs for consistency in sample preparation, the avoidance of spectroscopic artefacts and an appreciation of the subtleties of the interpretation of EPR spectra. The latter often only receive limited attention when EPR is only one of a number of complementary techniques. In the end, the desired outcome is a picture of the structure of the active site that leads directly to an understanding of how and why it functions as a neurobiologically active centre. Such an understanding is important for a rational approach to therapeutic strategies or palliative treatments for neurodegenerative diseases. As is the case with all biophysical studies, we should endeavour to correlate these with physiological and pathological studies and be very aware of the limitations of the data when this is impossible.

References

Abragam A, Bleaney B (1970) Electron paramagnetic resonance of transition ions. Clarendon Press, Oxford

Antzutkin ON (2004) Amyloidosis of Alzheimer's Abeta peptides: solid-state nuclear magnetic resonance, electron paramagnetic resonance, transmission electron microscopy, scanning transmission electron microscopy and atomic force microscopy studies. Magn Reson Chem 42:231–246

Antzutkin ON, Balbach JJ, Leapman RD, Rizzo NW, Reed J, Tycko R (2000) Multiple quantum solid-state NMR indicates a parallel, not antiparallel, organization of β-sheets in Alzheimer's β-amyloid fibrils. Proc Natl Acad Sci 97:13045–13050

Barnham KJ, Ciccotosto GD, Tickler AK, Ali FE, Smith DG, Williamson NA, Lam YH, Carrington D, Tew D, Kocak G, Volitakis I, Separovic F, Barrow CJ, Wade JD, Masters CL, Cherny RA, Curtain CC, Bush AI, Cappai R (2003a) Neurotoxic, redox-competent Alzheimer's beta-amyloid is released from lipid membrane by methionine oxidation. J Biol Chem 278:42959–42965

Barnham KJ, McKinstry WJ, Multhaup G, Galatis D, Morton CJ, Curtain CC, Williamson NA, White AR, Hinds MG, Norton RS, Beyreuther K, Masters CL, Parker MW, Cappai R (2003b) Structure of the Alzheimer's disease amyloid precursor protein copper binding domain. A regulator of neuronal copper homeostasis. J Biol Chem 278:17401–17407

Barnham KJ, Haeffner F, Ciccotosto GD, Curtain CC, Tew D, Mavros C, Beyreuther K, Carrington D, Masters CL, Cherny RA, Cappai R, Bush AI (2004) Tyrosine gated electron transfer is the key to the toxic mechanism of Alzheimer's disease β-amyloid. FASEB J 18:1427–1429

Bayer TA, Jakala P, Hartmann T, Havas L, McLean C, Culvenor JG, Li QX, Masters CL, Falkai P, Beyreuther K (1999) Alpha-synuclein accumulates in Lewy bodies in Parkinson's disease and dementia with Lewy bodies but not in Alzheimer's disease beta-amyloid plaque cores. Neurosci Lett 266:213–216

Bencini A, Gatteschi D (1990) EPR of exchange coupled systems. Springer, Berlin

Berliner LJ (1983) The spin-label approach to labeling membrane protein sulfhydryl groups. Ann N Y Acad Sci 414:153–161

Bleaney B, Bowers KD, Pryce MHL (1955) Paramagnetic resonance in diluted copper salts III. Theory and evaluation of the nuclear electric quadrupole moments of ^{63}Cu and ^{65}Cu. Proc R Soc (London) A228:166–174

Brown DR (2007) Interactions between metals and α-synuclein—function or artefact? FEBS J 274:3766–3774

Brown DR, Kozlowski H (2004) Biological inorganic and bioinorganic chemistry of neurodegeneration based on prion and Alzheimer diseases. Dalton Trans 1907–1917

Brown LJ, Sale KL, Hills R, Rouviere C, Song L, Zhang X, Fajer PG (2002) Structure of the inhibitory region of troponin by site directed spin labeling electron paramagnetic resonance. Proc Natl Acad Sci USA 99:12765–12770

Burns CS, Aronoff-Spencer E, Legname G, Prusiner SB, Antholine WE, Gerfen GJ, Peisach J, Millhauser GL (2003) Copper coordination in the full-length, recombinant prion protein. Biochemistry 42:6794–6803

Cherny RA, Atwood CS, Xilinas ME, Gray DN, Jones WD, McLean CA, Barnham KJ, Volitakis I, Fraser FW, Kim Y, Huang X, Goldstein LE, Moir RD, Lim JT, Beyreuther K, Zheng H, Tanzi RE, Masters CL, Bush AI (2001) Treatment with a copper-zinc chelator markedly and rapidly inhibits beta-amyloid accumulation in Alzheimer's disease transgenic mice. Neuron 30:665–676

Ciccotosto GD, Tew D, Curtain CC, Smith D, Carrington D, Masters CL, Bush AI, Cherny RA, Cappai R, Barnham KJ (2004) Enhanced toxicity and cellular binding of a modified amyloid beta peptide with a methionine to valine substitution. J Biol Chem 279:42528–42534

Collinge J, Whitfield J, McKintosh E, Beck J, Mead S, Thomas DJ, Alpers MP (2006) Kuru in the 21st century—an acquired human prion disease with very long incubation periods. Lancet 367:2068–2074

Curtain CC, Ali F, Volitakis I, Cherny RA, Norton RS, Beyreuther K, Barrow CJ, Masters CL, Bush AI, Barnham KJ (2001) Alzheimer's disease amyloid-beta binds copper and zinc to generate an allosterically ordered membrane-penetrating structure containing superoxide dismutase-like subunits. J Biol Chem 276:20466–20473

Curtain CC, Ali FE, Smith DG, Bush AI, Masters CL, Barnham KJ (2003) Metal ions, pH, and cholesterol regulate the interactions of Alzheimer's disease amyloid-beta peptide with membrane lipid. J Biol Chem 278:2977–2982

Deligiannakis Y, Louloudi M, Hadjiliadis N (2000) Electron spin echo envelope modulation (ESEEM) spectroscopy as a tool to investigate the coordination environment of metal centers. Coord Chem Rev 204:1–112

Der-Sarkissian A, Jao CC, Chen J, Langen R (2003) Structural organization of alpha-synuclein fibrils studied by site-directed spin labeling. J Biol Chem 278:37530–37535

Dong J, Canfield JM, Mehta AK, Shokes JE, Tian B, Childers WS, Simmons JA, Mao Z, Scott RA, Warncke K, Lynn DG (2007) Engineering metal ion coordination to regulate amyloid fibril assembly and toxicity. Proc Natl Acad Sci (USA) 104:13313–13318

Drew S, Barnham K (2007) Investigations of the prion protein using electron paramagnetic resonance. In: Hill AF (ed) Methods of molecular biology. Humana Press, New Jersey

Ehmann WD, Markesbery WR, Alauddin M, Hossain TI, Brubaker EH (1986) Brain trace elements in Alzheimer's disease. Neurotoxicology 7:195–206

Froncisz W, Hyde JS (1980) Broadening by strains in the *g* parallel region of Cu^{2+} EPR spectra. J Chem Phys 73:3123–3131

Gajdusek DC, Gibbs CJ Jr, Alpers M (1967) Transmission and passage of experimental "kuru" to chimpanzees. Science 155:212–214

Guilloreau L, Damian L, Coppel Y, Mazarguil Y, Winterhalter M, Faller P (2006) Structural and thermodynamical properties of CuII amyloid-β16/28 complexes associated with Alzheimer's disease. J Biol Inorg Chem 11:1024–1038

Haddad MS, Hendrickson DN (1978) Magnetic exchange interactions in binuclear transition-metal complexes. 15. Copper (II) and nickel (II) complexes bridged by imidazolate, benzimidazolate, biimidazolate, and bibenzimidazolate ions. Inorg Chem 17:2622–2630

Hanson GR, Gates KE, Noble CJ, Griffin M, Mitchell A, Benson S (2004) XSophe-Sophe-XeprView®. A computer simulation software suite (v.1.1.3) for the analysis of continuous wave EPR spectra. J Inorg Biochem 98:903–916

Hodgson DJ (1975) The structural and magnetic properties of first-row transition-metal dimers containing hydroxo, substituted hydroxo, and halogen bridges. Prog Inorg Chem 19:173–241

Huang X, Atwood CS, Moir RD, Hartshorn MA, Vonsattel JP, Tanzi RE, Bush AI (1997) Zinc-induced Alzheimer's Abeta 1–40 aggregation is mediated by conformational factors. J Biol Chem 272:26464–26470

Huang X, Cuajungco MP, Atwood CS, Hartshorn MA, Tyndall JD, Hanson GR, Stokes KC, Leopold M, Multhaup G, Goldstein LE, Scarpa RC, Saunders AJ, Lim J, Moir RD, Glabe C, Bowden EF, Masters CL, Fairlie DP, Tanzi RE, Bush AI (1999) Cu(II) potentiation of alzheimer abeta neurotoxicity. Correlation with cell-free hydrogen peroxide production and metal reduction. J Biol Chem 274:37111–37116

Inanami O, Hashida S, Iizuka D, Horiuchi M, Hiraoka W, Shimoyama Y, Nakamura H, Inagaki F, Kuwabara M (2005) Conformational change in full-length mouse prion: a site-directed spin-labeling study. Biochem Biophys Res Commun 335:785–792

Karr JW, Szalai VA (2007) Role of aspartate-1 in Cu(II) binding to the amyloid-beta peptide of Alzheimer's disease. J Am Chem Soc 129:3796–3797

Karr JW, Kaupp LJ, Szalai VA (2004) Amyloid-beta binds Cu^{2+} in a mononuclear metal ion binding site. J Am Chem Soc 126:13534–13538

Karr JW, Akintoye H, Knapp LJ, Scalia VA (2005) N-Terminal deletions modify the Cu^{2+} binding site in amyloid-beta. Biochemistry 44:5478–5487

Kong GK, Adams JJ, Harris HH, Boas JF, Curtain CC, Galatis D, Masters CL, Barnham KJ, McKinstry WJ, Cappai R, Parker MW (2007) Structural studies of the Alzheimer's amyloid precursor protein copper-binding domain reveal how it binds copper ions. J Mol Biol 367:148–161

Kowalik-Jankowska T, Ruta-Dolejsz M, Wisniewska K, Lankiewicz L (2002) Coordination of copper (II) ions by the 11–20 and 11–28 fragments of human and mouse beta-amyloid peptide. J Inorg Biochem 92:1–10

Kowalik-Jankowska T, Ruta M, Wisniewska K, Lankiewicz L (2003) Coordination abilities of the 1–16 and 1–28 fragments of beta-amyloid peptide towards copper (II) ions: a combined potentiometric and spectroscopic study. J Inorg Biochem 95:270–272

Kowalik-Jankowska T, Rajewska A, Wisniewska K, Grzonka Z, Jezierska J (2005) Coordination abilities of N-terminal fragments of α-synuclein towards copper (II) ions: a combined potentiometric and spectroscopic study. J Inorg Biochem 99:2282–2291

Lovell MA, Robertson JD, Teesdale WJ, Campbell JL, Markesbery WR (1998) Copper, iron and zinc in Alzheimer's disease senile plaques. J Neurol Sci 158:47–52

Lue LF, Kuo YM, Roher AE, Brachova L, Shen Y, Sue L, Beach T, Kurth JH, Rydel RE, Rogers J (1999) Soluble amyloid beta peptide concentration as a predictor of synaptic change in Alzheimer's disease. Am J Pathol 155:853–862

Lundberg KM, Stenland CJ, Cohen FE, Prusiner SB, Millhauser GL (1997) Kinetics and mechanism of amyloid formation by the prion protein H1 peptide as determined by time-dependent ESR. Chem Biol 4:345–355

Maki AH, McGarvey BR (1958) Electron spin resonance in transition metal chelates. I. Copper (II) bis-acetylacetonate. J Chem Phys 29:31–34

McCracken J, Pember S, Benkovic SJ, Villafranca JJ, Miller RJ, Peisach J (1988) Electron spin-echo studies of the copper binding site in phenylalanine hydroxylase from *Chromobacterium violaceum*. J Am Chem Soc 110:1069–1074

McLean CA, Cherny RA, Fraser FW, Fuller SJ, Smith MJ, Beyreuther K, Bush AI, Masters CL (1999) Soluble pool of Abeta amyloid as a determinant of severity of neurodegeneration in Alzheimer's disease. Ann Neurol 46:860–866

Miura T, Suzuki K, Kohata N, Takeuchi H (2000) Metal binding modes of Alzheimer's amyloid β- peptide in insoluble aggregates and soluble complexes. Biochemistry 39:7024–7031

Narayanan S, Reif B (2005) Characterization of chemical exchange between soluble and aggregated states of beta amyloid by solution-state NMR upon variation of salt conditions. Biochemistry 44:1444–1452

Ohtsu H, Shimazaki Y, Odani A, Yamauchi O, Mori W, Itoh S, Fukuzumi S (2000) Synthesis and characterization of imidozolate-bridged dinuclear complexes as active site models of Cu, Zn-SOD. J Am Chem Soc 122:5733–5741

Paik SR, Shin H-J, Lee J-H, Chang C-S, Kim J (1999) Copper (II)-induced self-oligomerization of α-synuclein. Biochem J 340:821–828

Peisach J, Blumberg WE (1974) Structural implications derived from the analysis of electron paramagnetic resonance spectra of natural and artificial copper proteins. Arch Biochem Biophys 165:691–708

Pilbrow JR (1990) Transition ion electron paramagnetic resonance. Clarendon Press, Oxford

Rasia RM, Bertoncini CW, Marsh D, Hoyer W, Cherny D, Zweckstetter M, Griesinger C, Jovin TM, Fernandez CO (2005) Structural characterization of copper (II) binding to alpha-synuclein: insights into the bioinorganic chemistry of Parkinson's disease. Proc Natl Acad Sci USA 102:4294–4299

Ritchie CW, Bush AI, Mackinnon A, Macfarlane S, Mastwyk M, MacGregor L, Kiers L, Cherny R, Li QX, Tammer A, Carrington D, Mavros C, Volitakis I, Xilinas M, Ames D, Davis S, Beyreuther K, Tanzi RE, Masters CL (2003) Metal-protein attenuation with iodochlorhydroxyquin (clioquinol) targeting Abeta amyloid deposition and toxicity in Alzheimer disease: a pilot phase 2 clinical trial. Arch Neurol 60:1685–1691

Smith TD, Pilbrow JR (1974) The determination of structural properties of dimeric transition metal complexes from EPR spectra. Coord Chem Rev 13:173–278

Smith DP, Smith DG, Curtain CC, Boas JF, Pilbrow JR, Ciccotosto GD, Lau TL, Tew DJ, Perez K, Wade JD, Bush AI, Drew SC, Separovic F, Masters CL, Cappai R, Barnham KJ (2006) Copper-mediated amyloid-beta toxicity is associated with an intermolecular histidine bridge. J Biol Chem 281:15145–15154

Smith DP, Ciccotosto GD, Tew DJ, Fodero-Tavoletti MT, Johanssen T, Masters CL, Barnham KJ, Cappai R (2007) Concentration dependent Cu^{2+} induced aggregation and dityrosine formation of the Alzheimer's disease amyloid-beta peptide. Biochemistry 46:2881–2891

Stellato F, Menestrina G, Dalla Serra M, Potrich C, Tomazzolli R, Meyer-Klaucke W, Morante S (2006) Metal binding in amyloid β-peptides shows intra- and inter-peptide coordination modes. Eur Biophys J 35:340–351

Sung Y, Rospigliosi C, Eliezer D (2006) NMR mapping of copper binding sites in alpha-synuclein. Biochim Biophys Acta 1764:5–12

Syme CD, Nadal RC, Rigby SE, Viles JH (2004) Copper binding to the amyloid-beta (Abeta) peptide associated with Alzheimer's disease: folding, coordination geometry, pH dependence, stoichiometry, and affinity of Abeta-(1–28): insights from a range of complementary spectroscopic techniques. J Biol Chem 279: 18169–18177

Tickler AK, Smith DG, Ciccotosto GD, Tew DJ, Curtain CC, Carrinton D, Masters CL, Bush AI, Cherny RA, Cappai R, Wade JD, Barnham KJ (2005) Methylation of the imidazole side chain of the Alzheimer disease amyloid-β peptide results in abolition of superoxide dismutase-like structures and inhibition of neurotoxicity. J Biol Chem 280:13355–13363

Valensin D, Mancini FM, Luczkowski M, Janicka A, Wisniewska K, Gaggelli E, Valensin G, Lankiewicz L, Kozlowski H (2004) Identification of a novel high affinity copper binding site in the APP (145–155) fragment of amyloid precursor protein. Dalton Trans 16–22

Van Doorslaer S, Cereghetti GM, Glockshuber R, Schweiger A (2001) Unlocking the Cu^{2+} binding sites in the C-terminal domain of the murine prion protein: a pulse EPR and ENDOR study. J Phys Chem B 105:1631–1639

Van Vleck J (1948) Theory of the width of microwave lines in cupric salts. Phys Rev 73:1249–1250

Watanabe Y, Inanami O, Horiuchi M, Hiraoka W, Shimoyama Y, Inagaki F, Kuwabara M (2006) Identification of pH-sensitive regions in the mouse prion by the cysteine-scanning spin-labeling ESR technique. Biochem Biophys Res Commun 350: 549–556

Weil JA, Bolton JR, Wertz JE (1994) Electron paramagnetic resonance. Elementary theory and practical applications. Wiley-Interscience, New York

Wood SJ, Wypych J, Steavenson S, Louis JC, Citron M, Biere AL (1999) Alpha-synuclein fibrillogenesis is nucleation-dependent. Implications for the pathogenesis of Parkinson's disease. J Biol Chem 274:19509–19512

Yokoi H, Addison AW (1977) Spectroscopic and redox properties of pseudotetrahedral copper (II) complexes. Their relationship to copper proteins. Inorg Chem 16:1341–1349